International Communications in Heat and Mass Transfer 126 (2021) 105484

Contents lists available at ScienceDirect

International Communications in Heat and Mass Transfer

journal homepage: www.elsevier.com/locate/ichmt

Dynamics of water conveying single-wall carbon nanotubes and magnetite nanoparticles subject to induced magnetic field: A bioconvective model for theranostic applications

S. Areekara [a], F. Mabood [b,*], A.S. Sabu [a], Alphonsa Mathew [a], I.A. Badruddin [c]

[a] Department of Mathematics, St. Thomas' College (Autonomous), Thrissur 680001, Kerala, India
[b] Department of Information Technology, Fanshawe College, London, ON, Canada
[c] Department of Mechanical Engineering, College of Engineering, King Khalid University, Asir, Abha 61421, Saudi Arabia

ARTICLE INFO

Keywords:
Hybrid nanofluid
Induced magnetic field
Stagnation point flow
Stratification
Microorganisms

ABSTRACT

The current study presents a bioconvective model to investigate the dynamics of water conveying single-wall carbon nanotubes (SWCNTs) and magnetite nanoparticles on the stagnation point flow along a stretching sheet subject to chemical reaction, viscous dissipation, induced magnetic field, and stratification effects. With applications ranging from biomedical imaging, hyperthermia, targeted drug delivery, and cancer therapy, the present study provides a theoretical perspective that is beneficial in biomedical engineering. Relevant similarity formulas are effectuated in converting the governing equations into a system of ODEs and are further treated numerically using the Runge-Kutta-Fehlberg method with the shooting technique. Illustrations on the effect of temperature, microorganisms, concentration, and velocity profiles due to the varying parameter values are achieved with the aid of graphs. It is observed that augmenting volume fraction of single-wall carbon nanotube and magnetite nanoparticles exhibit a constructive effect on temperature profile, which helps in killing cancerous cells. Further, the simultaneous impact of effectual parameters on surface drag, heat transfer rate, mass transfer rate, and microorganism density number is studied using graphs. It is seen that augmenting chemical reaction parameter tends to elevate the mass transfer rate and the microorganism density number.

1. Introduction

The use of nanofluid in place of conventional fluid by Choi [1] marked a major breakthrough in the field of fluid dynamics. Since then, scientists have been working hard to further enhance heat transfer capabilities. Studies dealing with various nanofluids can be seen in [2–5]. Mass and heat transfer plays a pivotal role in many aspects of engineering and medical field. Fluids constituting two or more nanoparticles are termed hybrid nanofluids. Mabood et al. [6] investigated the significance of melting heat transfer, magnetic field, and nonlinear radiation on hybrid nanoliquid flow over a stretched surface and observed that augmenting nanoparticle volume fraction of copper tends to increase the heat transfer rate. The consequence of the Newtonian heating process and nonlinear thermal radiation effect on water-based $Cu - Ti_2O_3$ hybrid nanofluid flow over an elongating porous surface considering Darcy-Forchheimer's model was analyszed by Yusuf et al. [7]. They noticed that the rate of entropy generation upsurged for ordinary nanofluid when compared with the hybrid nanofluid. Jakeer and Reddy [8] examined the impact of viscous dissipation, heat generation, and slip on the entropy generation in electro-magnetohydrodynamic (EMHD) $Ag - Cu - H_2O$ hybrid nanofluid. In addition, Zainal et al. [9] explored the unsteady EMHD stagnation point flow in a hybrid nanofluid concerning a stretching/shrinking sheet. A few more studies dealing with hybrid nanofluids can be seen in [10–12].

The magnetic field represents an important characteristic of hydromagnetic problems. In some cases, the magnetic Reynolds number of the flow may not be realistic to be assumed small in magnitude; hence induced magnetic field (the additional magnetic field that gets induced on electrically conducting fluid in the presence of an external magnetic field.) is not negligible (see [13]). However, studies incorporating induced magnetic field effects are limited in number. Kumari et al. [14] numerically explored the impact of induced magnetic field on heat transfer over a lengthening sheet. Ali et al. [15] used the Keller-box method to numerically analyze the steady MHD boundary layer flow over an elongating sheet considering induced magnetic field and

* Corresponding author.
E-mail address: mabood1971@yahoo.com (F. Mabood).

https://doi.org/10.1016/j.icheatmasstransfer.2021.105484

Available online 15 July 2021

Nomenclature

a, c	Dimensional constants
W_c	Maximum cell swimming speed
Ec	Eckert number
N	Microorganism concentration
C	Fluid concentration
T	Fluid temperature (K)
N_W	Concentration of microorganism near the wall
C_W	Nanoparticle concentration near the wall
T_W	Wall fluid temperature
Cf_x	Local drag coefficient
Lb	Bioconvection Lewis number
k_r	Reaction rate constant (s^{-1})
b	Chemotaxis constant
D_B	Chemical molecular diffusivity (m^2s^{-1})
Kr	Chemical reaction parameter
Pr	Prandtl number
C_p	Specific heat
Pe	Peclet number
Nn_x	Local motile density
Sh_x	Local Sherwood number
Nu_x	Local Nusselt number
H_e	Magnetic field at free stream
D_m	Microorganism diffusion coefficient (m^2s^{-1})
x, y	Cartesian coordinates (m)
s_1, s_2, s_3	Stratification parameters
Le	Lewis number
u, v	Velocity components (ms^{-1})
H_0	Uniform magnetic field at infinity (Am^{-1})
T_∞	Ambient fluid temperature
C_∞	ambient nanoparticle concentration
C_0	Reference nanoparticle concentration
T_0	Reference temperature
N_0	Reference concentration of microorganism
N_∞	Ambient concentration of microorganism

Greek symbols

ϑ	Kinematic viscosity (m^2s^{-1})
ζ	Dimensionless variable
μ	Dynamic viscosity
λ	Reciprocal of magnetic Prandtl number
μ_e	Magnetic permeability ($kg\ m\ s^{-2}\ A^{-2}$)
α_m	Magnetic diffusivity (m^2s^{-1})
ρ	Density of the fluid (kgm^{-3})
κ	Thermal conductivity ($Wm^{-1}K^{-1}$)
ϕ	Nanoparticle volume fraction
σ	Electrical conductivity ($kg^{-1}\ m^{-3}\ s^3\ A^2$)
β	Magnetic parameter
α	Thermal diffusivity (m^2s^{-1})
Ω	Microorganism concentration difference parameter

Subscripts

hnf	Hybrid nanofluid
nf	Nanofluid
f	Conventional fluid

observed an increase in Nusselt number with magnetic parameter. Iqbal et al. [16] carried out investigations on entropy generation and induced magnetic field effects on Cu and TiO_2 nanofluid using Keller box method and noted an improved thermal conductivity for water based TiO_2 nanofluid when compared with water based Cu nanofluid.

The stagnation point corresponds to the point where the fluid's local velocity is zero. Nanofluid studies incorporating microorganisms is a developing field that has fascinated countless researchers due to its relevance in antibiotics, toxin removal, biofuel, targeted drug delivery and food digestion. Ali et al. [17] extended the work of Mahapatra and Gupta [18] to analyze the hydromagnetic stagnation point flow of an electrically conducting fluid over a lengthening sheet in the presence of an induced magnetic field. Later, Junoh et al. [19] extended the work of Ali et al. [17] by considering the stagnation point flow past a stretching/shrinking sheet in a hybrid nanomaterial.

CNT (carbon nanotube) is a graphene sheet rolled up into a tube having a nanoscale diameter. They are categorised into MWCNT (multi-wall carbon nanotubes) and SWCNT (single-wall carbon nanotubes) based on the number of used graphene sheets. CNT finds its use in device modelling, structural reinforcement, electromagnetic shields, automotive parts, energy storage, etc. CNTs are also administered in drug delivery, delivery of genetic material, cancer diagnosis & treatment, thermal ablation, etc. Ijaz et al. [20] elucidated the impact of CNTs on stagnation flow over a stretched surface involving quartic chemical reaction and induced magnetic field. Iqbal et al. [21] conducted a numerical investigation to exploit the response of induced magnetic field on transfer quantities using MWCNT and SWCNT and noted a constructive effect for nanoparticle volume fraction on the induced magnetic field. Some neoteric studies concerning CNTs are given in [22–26]. The current work concentrates on SWCNTs and not on MWCNTs due to the amelioration it provides in the medical field and also due to their lower toxicity level (see [27]).

The nanofluid studies involving microorganisms is an advancing field that has intrigued researchers due to its relevance in antibiotics, biofuel, toxin removal, targeted drug delivery and food digestion. Fluctuations in heat, mass and motile density profiles or the presence of different fluids trigger a formation of layers known as stratification. Bioconvection refers to the upward and downward movement of microorganisms caused by the unstable density stratification of microorganisms at the upper surface. Mehmood and Iqbal [28] utilized the fifth-order Runge-Kutta method to examine the consequence of induced magnetic field on stagnation point flow of nanofluid involving gyrotactic microorganisms. Further, *Al*-Amri and Muthtamilselvan [29] explored the significance of thermal radiation, microorganisms, magnetic field, and activation energy on the two-dimensional stagnation point flow of an incompressible nanoliquid and noted an increase in the density of motile microorganisms for larger values of Peclet number. Ahmad et al. [30] numerically studied the consequence of magnetic field, double stratification, thermal radiation, activation energy, and heat generation on SWCNT and MWCNT nanoliquid flow past a wedge. A decline in the temperature profile is noted for augmenting thermal stratification parameter. Various articles exploring the effect of microorganisms and stratification are discussed in [31–34].

Motivated by previous studies, it is noted that the dynamics of water conveying single-wall carbon nanotubes and magnetite nanoparticles subject to induced magnetic field has not yet been studied. This paper attempts to fill this gap. Theranostics (a novel concept that involves the integration of diagnosis and therapy in a single platform) may be the specific applications of this research work (see [35–41]). The present work aims to:

- Construct the bioconvective model to study the dynamics of water conveying single-wall carbon nanotubes and magnetite nanoparticles considering induced magnetic field, thermal stratification, viscous dissipation, chemical reaction, solutal stratification, and motile density stratification effects.
- Provide theoretical knowledge on the consequence of effectual parameters on the flow profiles.

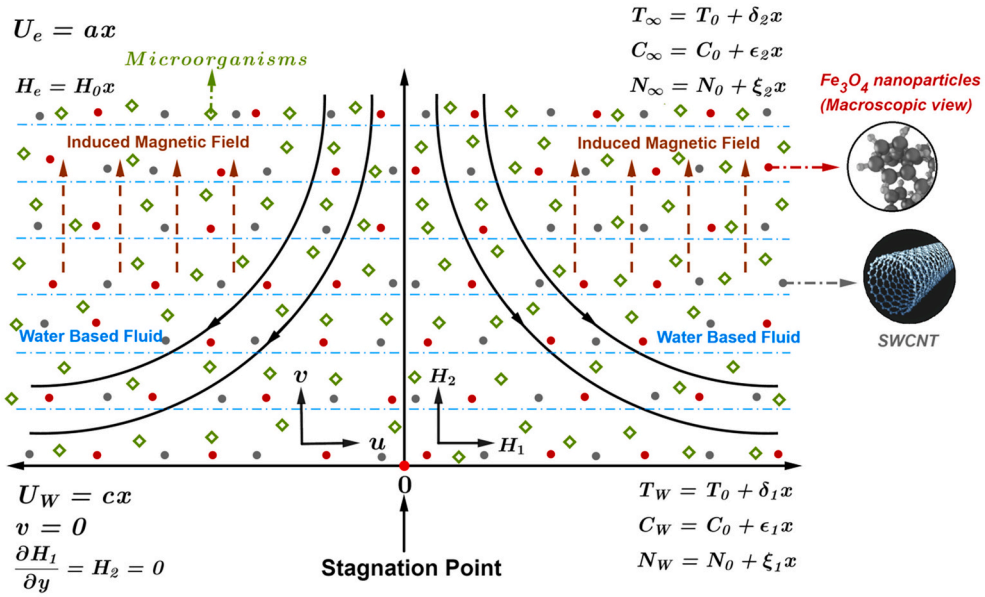

Fig. 1. Figurative representation.

- Explore the significance of pertinent parameters on surface drag, heat transfer rate, mass transfer rate, and microorganism density number.

2. Problem statement

Two-dimensional steady stagnation point flow over a linearly elongating sheet (Fig. 1) is considered under the ensuing assumptions:

(i) The expanding sheet is positioned along x *axis* and water-based Fe_3O_4 − *SWCNT* hybrid nanofluid containing microorganisms occupies the region $y > 0$.
(ii) $U_W(x) = cx$ and $U_e(x) = ax$ corresponds to the velocity of the lengthening sheet and the free stream, respectively.
(iii) Induced magnetic field vector, $H = (H_1, H_2)$ is considered with H_1 & H_2 being the magnetic integrants along x and y direction, respectively.
(iv) Chemical reaction and viscous dissipation effects are incorporated.
(v) Thermal, solutal and motile density stratification effects are also considered.

Governing equations takes the form (see [17,21,42]):

$$\frac{\partial u}{\partial x} + \frac{\partial v}{\partial y} = 0 \tag{1}$$

$$\frac{\partial \mathrm{H}_1}{\partial x} + \frac{\partial \mathrm{H}_2}{\partial y} = 0 \tag{2}$$

$$u\frac{\partial u}{\partial x} + v\frac{\partial u}{\partial y} - \frac{\mu_e}{4\pi\rho_{hnf}}\left(\mathrm{H}_1\frac{\partial \mathrm{H}_1}{\partial x} + \mathrm{H}_2\frac{\partial \mathrm{H}_1}{\partial y}\right) = U_e\frac{dU_e}{dx} - \frac{\mu_e \mathrm{H}_e}{4\pi\rho_{hnf}}\frac{d\mathrm{H}_e}{dx} + \left(\frac{\mu_{hnf}}{\rho_{hnf}}\right)\frac{\partial^2 u}{\partial y^2} \tag{3}$$

$$u\frac{\partial \mathrm{H}_1}{\partial x} + v\frac{\partial \mathrm{H}_1}{\partial y} - \mathrm{H}_1\frac{\partial u}{\partial x} - \mathrm{H}_2\frac{\partial u}{\partial y} = \alpha_m\frac{\partial^2 \mathrm{H}_1}{\partial y^2} \tag{4}$$

$$u\frac{\partial T}{\partial x} + v\frac{\partial T}{\partial y} = \alpha_{hnf}\frac{\partial^2 \mathrm{T}}{\partial y^2} + \frac{\mu_{hnf}}{(\rho C_p)_{hnf}}\left(\frac{\partial u}{\partial y}\right)^2 \tag{5}$$

$$u\frac{\partial C}{\partial x} + v\frac{\partial C}{\partial y} = D_B\frac{\partial^2 C}{\partial y^2} - k_r(C - C_\infty) \tag{6}$$

$$u\frac{\partial N}{\partial x} + v\frac{\partial N}{\partial y} + \frac{bW_c}{C_W - C_0}\left(\frac{\partial}{\partial y}\left(N\frac{\partial C}{\partial y}\right)\right) = D_m\frac{\partial^2 N}{\partial y^2} \tag{7}$$

with

$$\left.\begin{aligned} u = U_W(x) = cx, v = 0, \frac{\partial H_1}{\partial y} = H_2 = 0, \end{aligned}\right\} \; at\; y = 0$$

$$T = T_W = T_0 + \delta_1 x, C = C_W = C_0 + \epsilon_1 x, N = N_W = N_0 + \xi_1 x$$

$$\left.\begin{aligned} u \to U_e(x) = ax, H_1 \to H_e(x) = H_0 x, \end{aligned}\right\} \; as\; y \to \infty$$

$$T \to T_\infty = T_0 + \delta_2 x, C \to C_\infty = C_0 + \epsilon_2 x, N \to N_\infty = N_0 + \xi_2 x$$

where $\alpha_m = \frac{1}{4\pi\mu_e\sigma_{hnf}}$ represents the magnetic diffusivity.

Introducing the following similarity transformations (see [17,21,42]):

$$u = cxf'(\zeta), v = -\sqrt{c\vartheta_f}f(\zeta), H_1 = H_0 x g'(\zeta), H_2 = -H_0\sqrt{\frac{\vartheta_f}{c}}g(\zeta)$$

$$\zeta = y\sqrt{\frac{c}{\vartheta_f}}, \theta(\zeta) = \frac{T - T_\infty}{T_W - T_0}, \psi(\zeta) = \frac{C - C_\infty}{C_W - C_0}, \chi(\zeta) = \frac{N - N_\infty}{N_W - N_0}$$

into (1) − (7), we get:

$$f''' - A_1 A_2\left\{(f')^2 - ff'' - \frac{\beta}{A_2}\left\{(g')^2 - gg'' - 1\right\} - A^2\right\} = 0 \tag{8}$$

$$g'' - \frac{A_5}{\lambda}\left\{gf'' - fg''\right\} = 0 \tag{9}$$

$$\theta'' + \frac{A_3\, Pr}{A_4} f\, \theta' + \frac{Ec\, Pr}{A_1\, A_4} (f'')^2 = 0 \tag{10}$$

$$\psi'' + Le\, f\, \psi' - Kr\, Le\, \psi = 0 \tag{11}$$

$$\chi'' + Lb\, f\, \chi' - Pe\, \{ (\chi + \Omega)\, \psi'' + \chi'\, \psi' \} = 0 \tag{12}$$

subject to the boundary conditions:

$$\left. \begin{aligned} f(\zeta) = 0, f'(\zeta) = 1, g(\zeta) = 0, g'(\zeta) = 0, \end{aligned} \right\} when\ \zeta = 0$$

$$\theta(\zeta) = 1 - S_1, \psi(\zeta) = 1 - S_2, \chi(\zeta) = 1 - S_3$$

$$\left. \begin{aligned} f'(\zeta) \to A, g'(\zeta) \to 1, \theta(\zeta) \to 0, \psi(\zeta) \to 0, \chi(\zeta) \to 0 \end{aligned} \right\} as\ \zeta \to \infty$$

where the dimensionless parameters are:

$$A = \frac{a}{c}, \beta = \frac{\mu_e}{4\pi\rho_f} \left(\frac{H_0}{c}\right)^2, \lambda = \frac{1}{4\pi\mu_e \sigma_f \vartheta_f}, Pr = \frac{(\mu C_p)_f}{k_f} = \frac{\vartheta_f}{\alpha_f}$$

$$Le = \frac{\vartheta_f}{D_B}, Ec = \frac{(cx)^2}{(C_p)_f (T_W - T_0)}, Lb = \frac{\vartheta_f}{D_m}, Pe = \frac{bW_c}{D_m}$$

$$\Omega = \frac{N_\infty}{N_W - N_0}, Kr = \frac{k_r}{c}, S_1 = \frac{\delta_2}{\delta_1}, S_2 = \frac{\epsilon_2}{\epsilon_1}, S_3 = \frac{\xi_2}{\xi_1}$$

The nanofluid models incorporated are:

Physical quantities in the non-dimensional form are given by (see [21,42,44]):

Table 1
Comparison of drag coefficient ($Cf_x\, Re_x^{1/2}$) with [21,46,47] for different A values when $\phi_{Fe_3O_4} = \phi_{SWCNT} = \beta = \lambda = 0$

A	$Cf_x\, Re_x^{1/2}$			
	Iqbal et al. [21]	Hayat et al. [46]	Hayat et al. [47]	Present Results
0.1	−0.969386	−0.96939	−0.96937	−0.969386
0.2	−0.918107	−0.91811	−0.91813	−0.918107
0.5	−0.667263	−0.66726	−0.66723	−0.667264
0.7	−0.433475	−0.43346	−0.43345	−0.433476
0.8	−0.299388	−0.29929	−0.29921	−0.299389
0.9	−0.154716	−0.15458	−0.1545471	−0.154717
1	0	0	0	0.000000

Local drag coefficient: $Cf_x = \frac{\tau_\omega}{\rho_f (U_W)^2} = \frac{\mu_{hnf} \left.\frac{\partial u}{\partial y}\right|_{y=0}}{\rho_f (U_W)^2} \Rightarrow Cf_x\, Re_x^{1/2} = \frac{f''(0)}{A_1}$

Local Nusselt number: $Nu_x = \frac{x\, q_\omega}{\kappa_f (T_W - T_0)} = \frac{-x\, \kappa_{hnf} \left.\frac{\partial T}{\partial y}\right|_{y=0}}{\kappa_f (T_W - T_0)} \Rightarrow Nu_x\, Re_x^{-1/2} = -A_4\, \theta'(0)$

Local Sherwood number: $Sh_x = \frac{x\, q_m}{D_B (C_W - C_0)} = \frac{-x\, D_B \left.\frac{\partial C}{\partial y}\right|_{y=0}}{D_B (C_W - C_0)} \Rightarrow Sh_x\, Re_x^{-1/2} = -\psi'(0)$

Local microorganism density number: $Nn_x = \frac{x\, q_n}{D_m (N_W - N_0)} = \frac{-x\, D_m \left.\frac{\partial N}{\partial y}\right|_{y=0}}{D_m (N_W - N_0)} \Rightarrow Nn_x\, Re_x^{-1/2} = -\chi'(0)$ where $Re_x = \frac{U_W\, x}{\vartheta_f}$ is the local Reynold's number.

Hybrid Nanofluid Model (see [11,43–45])

$$\frac{\mu_{hnf}}{\mu_f} = \frac{1}{(1-\phi_{Fe_3O_4})^{2.5} (1-\phi_{SWCNT})^{2.5}} = \frac{1}{A_1}$$

$$\frac{\rho_{hnf}}{\rho_f} = (1-\phi_{SWCNT}) \left\{ (1-\phi_{Fe_3O_4}) + \frac{\rho_{Fe_3O_4}}{\rho_f} \phi_{Fe_3O_4} \right\} + \frac{\rho_{SWCNT}}{\rho_f} \phi_{SWCNT} = A_2$$

$$\frac{(\rho C_p)_{hnf}}{(\rho C_p)_f} = (1-\phi_{SWCNT}) \left\{ (1-\phi_{Fe_3O_4}) + \frac{(\rho C_p)_{Fe_3O_4}}{(\rho C_p)_f} \phi_{Fe_3O_4} \right\} + \frac{(\rho C_p)_{SWCNT}}{(\rho C_p)_f} \phi_{SWCNT} = A_3$$

$$\frac{k_{hnf}}{k_{bf}} = \frac{1 - \phi_{SWCNT} + 2\phi_{SWCNT} \left(\frac{k_{SWCNT}}{k_{SWCNT} - k_{bf}}\right) ln\left(\frac{k_{SWCNT} + k_{bf}}{2k_{bf}}\right)}{1 - \phi_{SWCNT} + 2\phi_{SWCNT} \left(\frac{k_{bf}}{k_{SWCNT} - k_{bf}}\right) ln\left(\frac{k_{SWCNT} + k_{bf}}{2k_{bf}}\right)}$$

$$\frac{k_{bf}}{k_f} = \frac{k_{Fe_3O_4} + 2k_f - 2\phi_{Fe_3O_4} (k_f - k_{Fe_3O_4})}{k_{Fe_3O_4} + 2k_f + \phi_{Fe_3O_4} (k_f - k_{Fe_3O_4})}$$

$$\frac{\sigma_{hnf}}{\sigma_f} = 1 + \frac{3 \left\{ \frac{\phi_{Fe_3O_4} \sigma_{Fe_3O_4} + \phi_{SWCNT} \sigma_{SWCNT}}{\sigma_f} - (\phi_{Fe_3O_4} + \phi_{SWCNT}) \right\}}{2 + \left\{ \frac{\phi_{Fe_3O_4} \sigma_{Fe_3O_4} + \phi_{SWCNT} \sigma_{SWCNT}}{(\phi_{Fe_3O_4} + \phi_{SWCNT}) \sigma_f} \right\} - \left\{ \frac{\phi_{Fe_3O_4} \sigma_{Fe_3O_4} + \phi_{SWCNT} \sigma_{SWCNT}}{\sigma_f} - (\phi_{Fe_3O_4} + \phi_{SWCNT}) \right\}}$$

$$A_4 = \frac{k_{hnf}}{k_f} \qquad A_5 = \frac{\sigma_{hnf}}{\sigma_f}$$

Nanofluid Model (see [21,44])

Effective Dynamic Viscosity : $\frac{\mu_{nf}}{\mu_f} = \frac{1}{(1-\phi_{Fe_3O_4})^{2.5}}$

Effective Density : $\frac{\rho_{nf}}{\rho_f} = (1-\phi_{Fe_3O_4}) + \phi_{Fe_3O_4} \left(\frac{\rho_{Fe_3O_4}}{\rho_f}\right)$

Effective Specific Heat : $\frac{(\rho C_p)_{nf}}{(\rho C_p)_f} = (1-\phi_{Fe_3O_4}) + \phi_{Fe_3O_4} \left(\frac{(\rho C_p)_{Fe_3O_4}}{(\rho C_p)_f}\right)$

Effective Thermal Conductivity : $\frac{\kappa_{nf}}{\kappa_f} = \frac{k_{Fe_3O_4} + 2k_f - 2\phi_{Fe_3O_4} (k_f - k_{Fe_3O_4})}{k_{Fe_3O_4} + 2k_f + \phi_{Fe_3O_4} (k_f - k_{Fe_3O_4})}$

Effective Electrical Conductivity : $\frac{\sigma_{nf}}{\sigma_f} = 1 + \frac{3\left(\frac{\sigma_{Fe_3O_4}}{\sigma_f} - 1\right)\phi_{Fe_3O_4}}{\left(\frac{\sigma_{Fe_3O_4}}{\sigma_f} + 2\right) - \left(\frac{\sigma_{Fe_3O_4}}{\sigma_f} - 1\right)\phi_{Fe_3O_4}}$

Table 2
Thermophysical properties [2,21,44] of water, Fe_3O_4 and SWCNT

Property	Water *(conventional fluid)*	Fe_3O_4 *(nanoparticle 1)*	SWCNT *(nanoparticle 2)*
ρ	997	5180	2600
C_p	4179	670	425
κ	0.613	9.7	6600
σ	0.05	25,000	10^6

3. Numerical scheme & validation

Eqs. (8) to (12) together with the boundary conditions shows a nonlinear nature and it seems to be difficult to find the closed-form or exact solution for the considered problem. Hence, the approximate solutions are computed numerically employing the Runge-Kutta-Fehlberg method cum shooting technique. This is accomplished by initially assuming:

$$\Upsilon_1 = f, \Upsilon_2 = f', \Upsilon_3 = f'', \Upsilon_3' = f''', \Upsilon_4 = g, \Upsilon_5 = g', \Upsilon_6 = g'', \Upsilon_6' = g''', \Upsilon_7 = \theta$$

$$\Upsilon_8 = \theta', \Upsilon_8' = \theta'', \Upsilon_9 = \psi, \Upsilon_{10} = \psi', \Upsilon_{10}' = \psi'', \Upsilon_{11} = \chi, \Upsilon_{12} = \chi', \Upsilon_{12}' = \chi''$$

The reduced system of first-order ODE is given by:

$$\Upsilon_1' = \Upsilon_2$$

$$\Upsilon_2' = \Upsilon_3$$

$$\Upsilon_3' = A_1 A_2 \left\{ (\Upsilon_2)^2 - \Upsilon_1 \Upsilon_3 - \frac{\beta}{A_2} \{(\Upsilon_5)^2 - \Upsilon_4 \Upsilon_6 - 1\} - A^2 \right\}$$

$$\Upsilon_4' = \Upsilon_5$$

$$\Upsilon_5' = \Upsilon_6$$

$$\Upsilon_6' = \frac{A_5}{\lambda} \{ \Upsilon_4 \Upsilon_3 - \Upsilon_1 \Upsilon_6 \}$$

$$\Upsilon_7' = \Upsilon_8$$

$$\Upsilon_8' = -\left\{ \frac{A_3 Pr}{A_4} \Upsilon_1 \Upsilon_8 + \frac{Ec\, Pr}{A_1 A_4} (\Upsilon_3)^2 \right\}$$

$$\Upsilon_9' = \Upsilon_{10}$$

$$\Upsilon_{10}' = Kr\, Le\, \Upsilon_9 - Le\, \Upsilon_1 \Upsilon_{10}$$

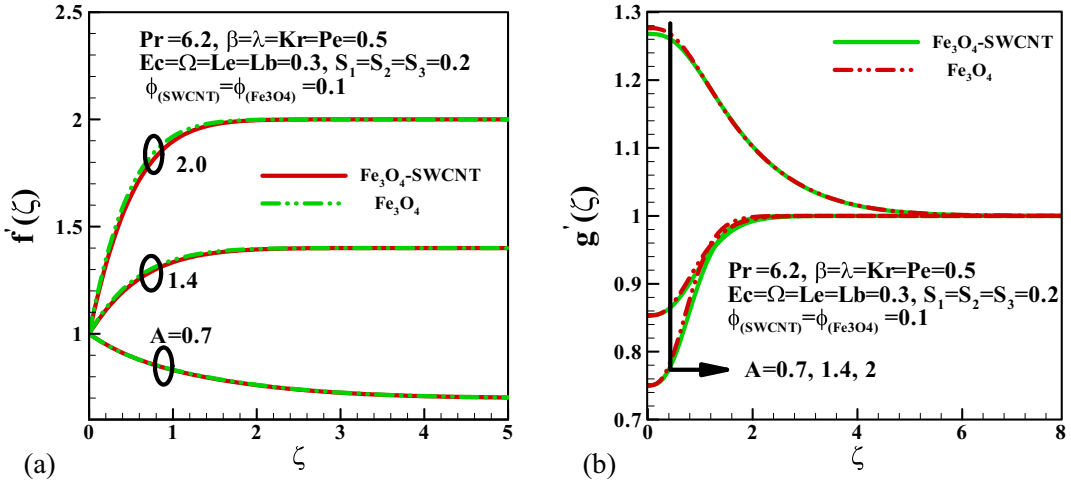

Fig. 2. Variation of A on $f'(\zeta)$ & $g'(\zeta)$.

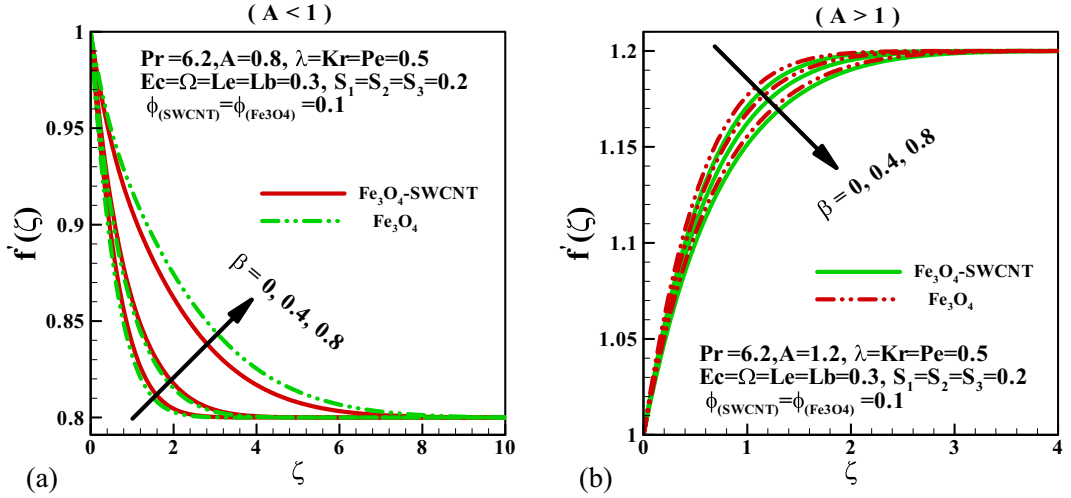

Fig. 3. Variation of β on $f'(\zeta)$.

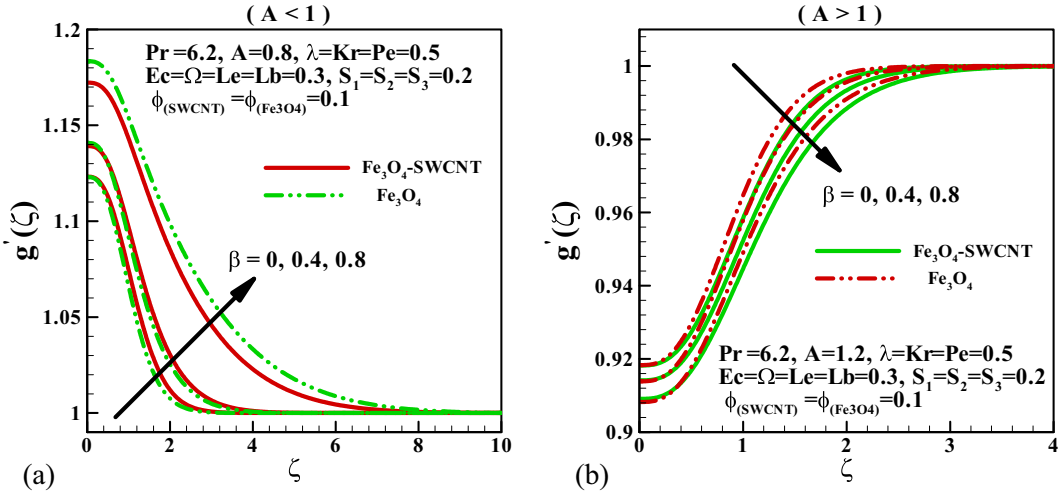

Fig. 4. Variation of β on $g'(\zeta)$.

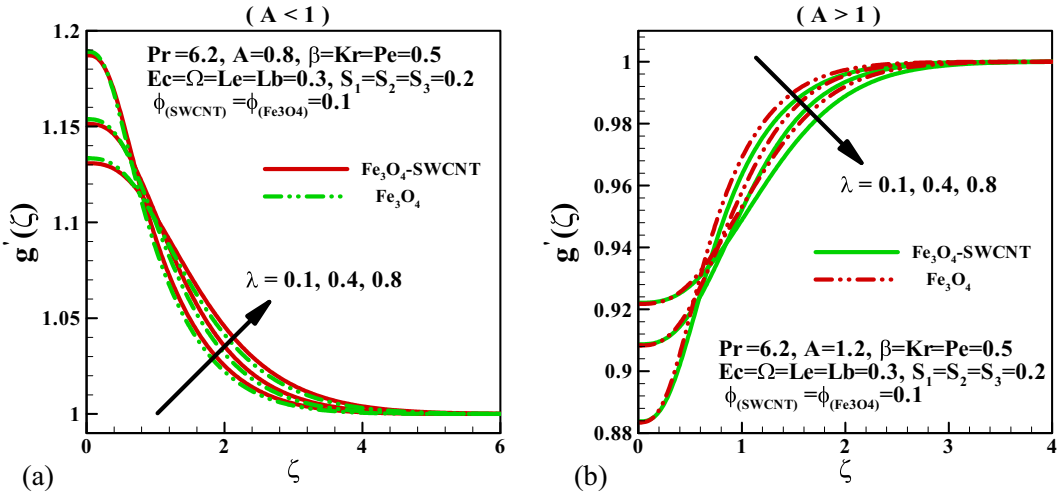

Fig. 5. Variation of λ on $g'(\zeta)$.

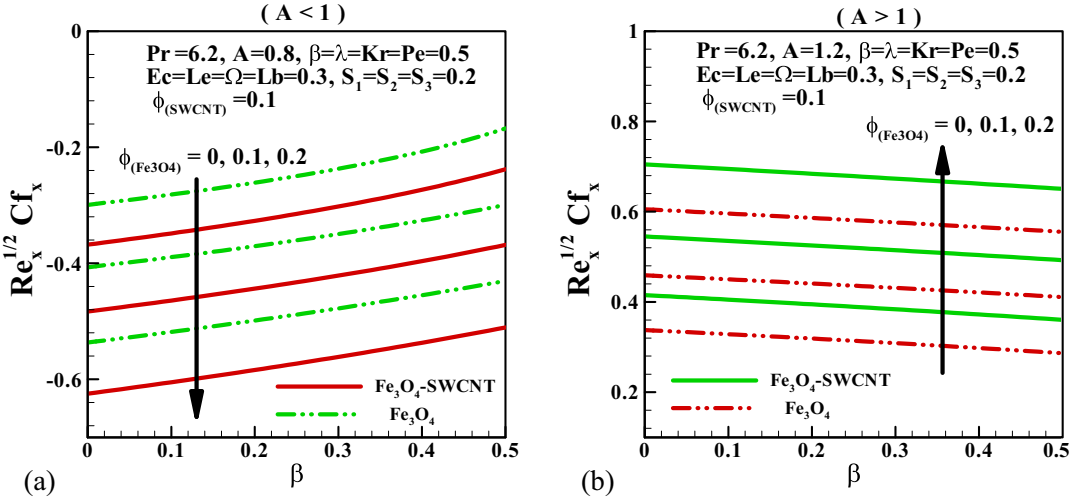

Fig. 6. Parallel effect of β *and* $\phi_{Fe_3O_4}$ on $Cf_x\, Re_x^{1/2}$.

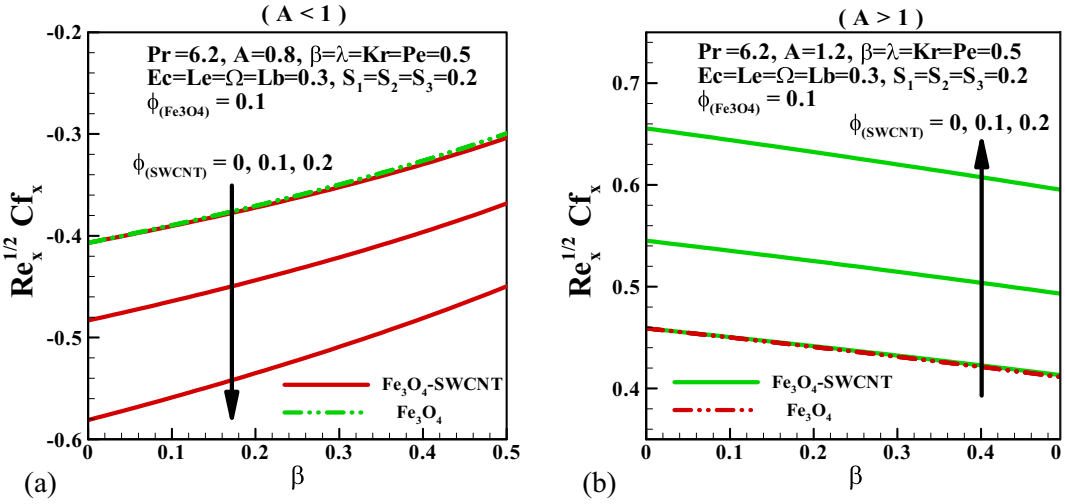

Fig. 7. Parallel effect of β *and* ϕ_{SWCNT} on $Cf_x\, Re_x^{1/2}$.

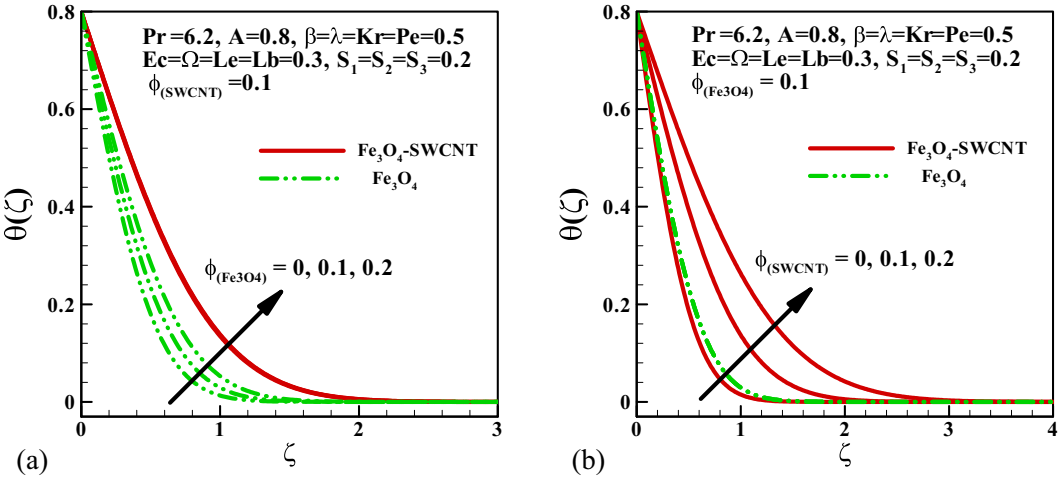

Fig. 8. Variation of $\phi_{Fe_3O_4}$ *and* ϕ_{SWCNT} on $\theta(\zeta)$.

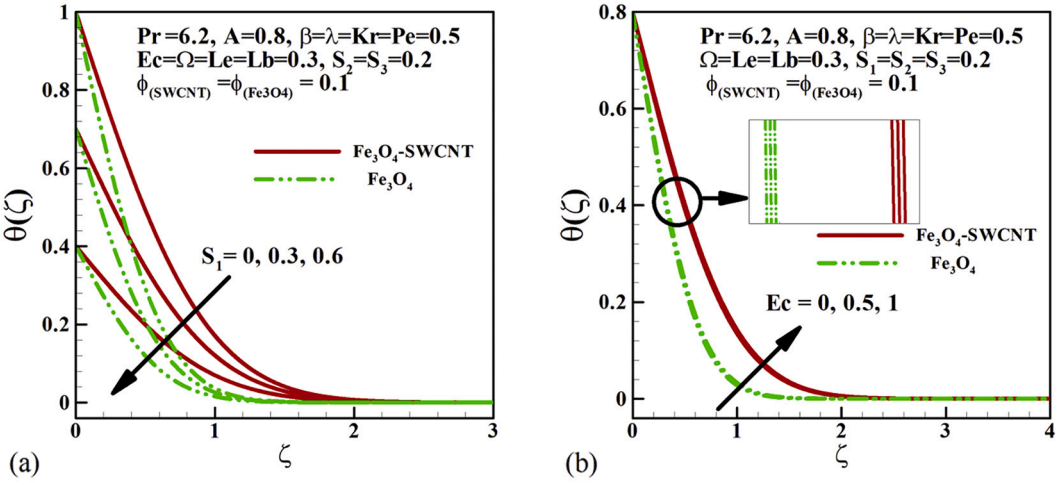

Fig. 9. Variation of S_1 *and* Ec on $\theta(\zeta)$.

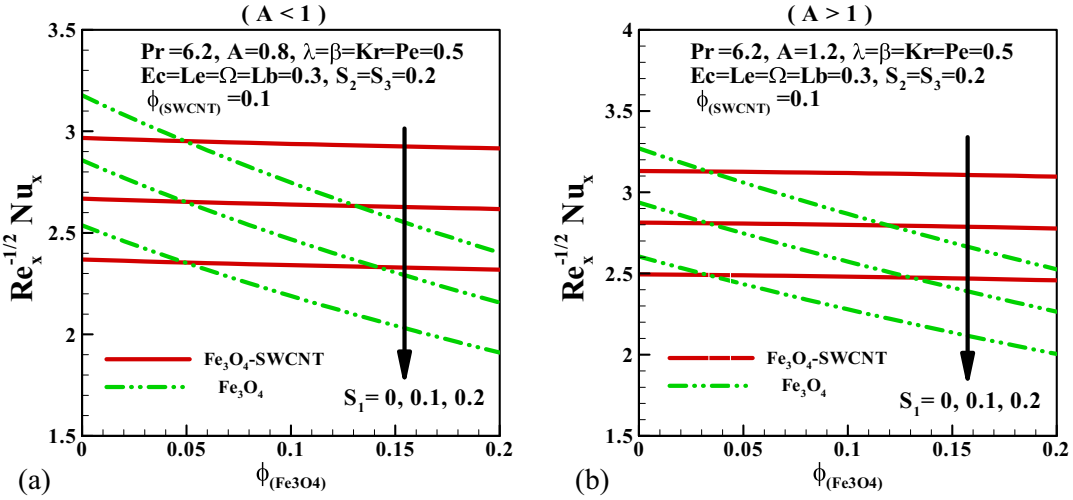

Fig. 10. Parallel effect of S_1 *and* $\phi_{Fe_3O_4}$ on $Nu_x\ Re_x^{-1/2}$.

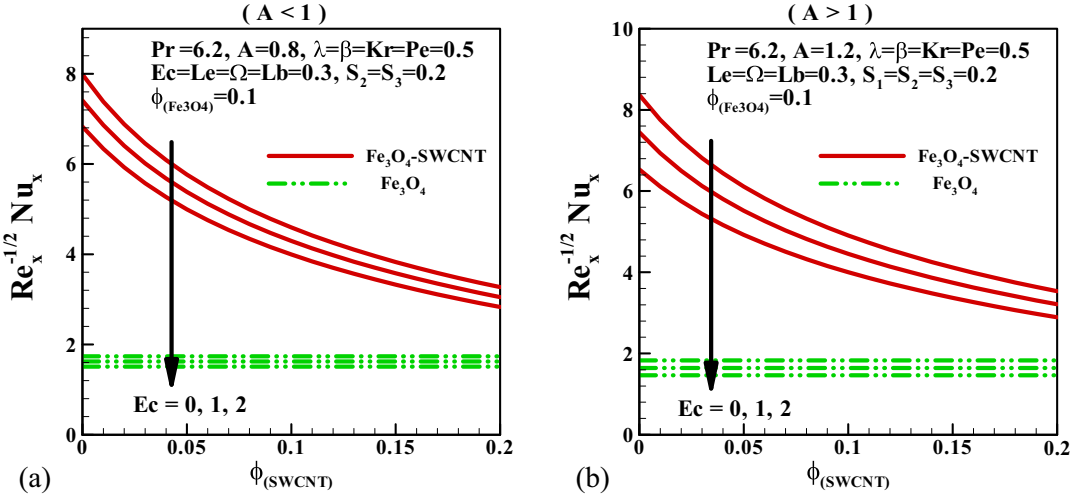

Fig. 11. Parallel effect of *Ec and* ϕ_{SWCNT} on $Nu_x\ Re_x^{-1/2}$.

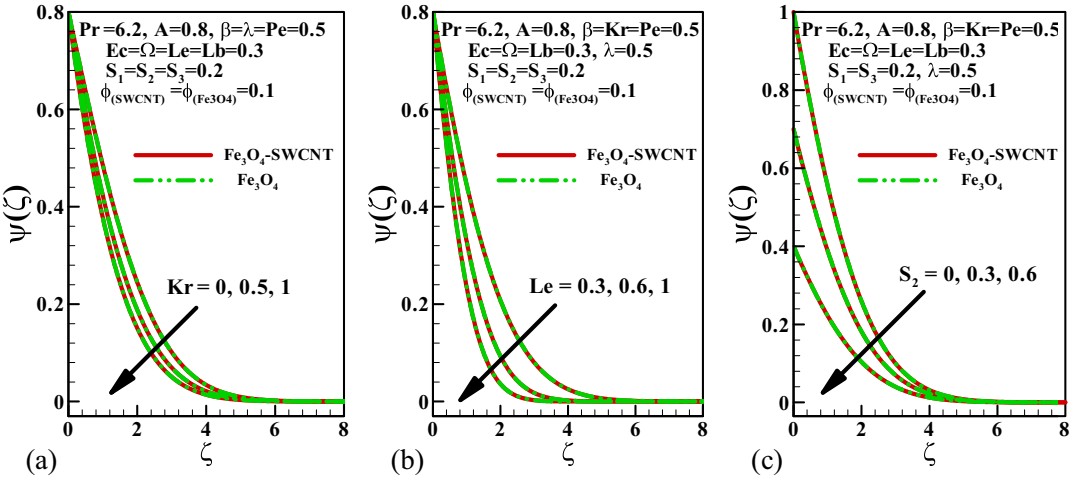

Fig. 12. Variation of *Kr, Le and* S_2 on $\psi(\zeta)$.

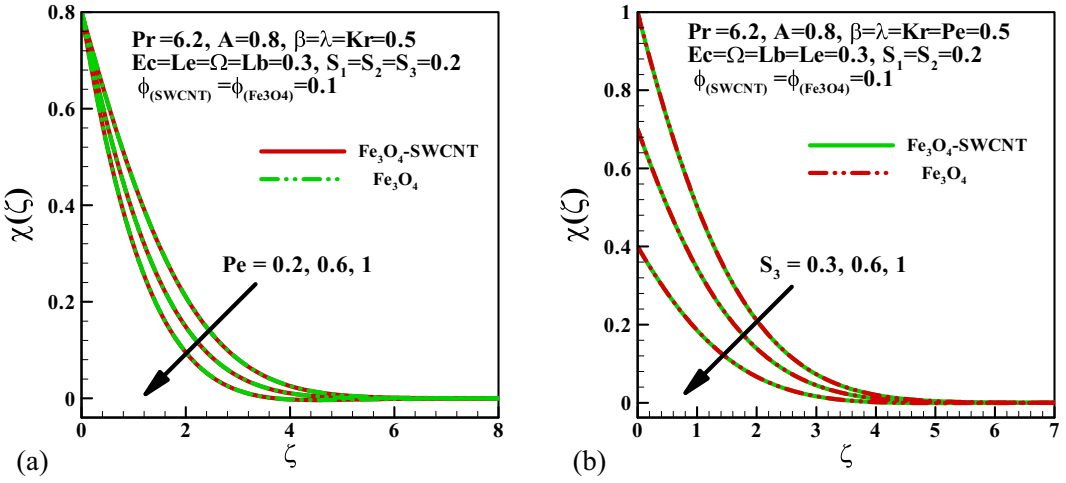

Fig. 13. Variation of *Pe and* S_3 on $\chi(\zeta)$.

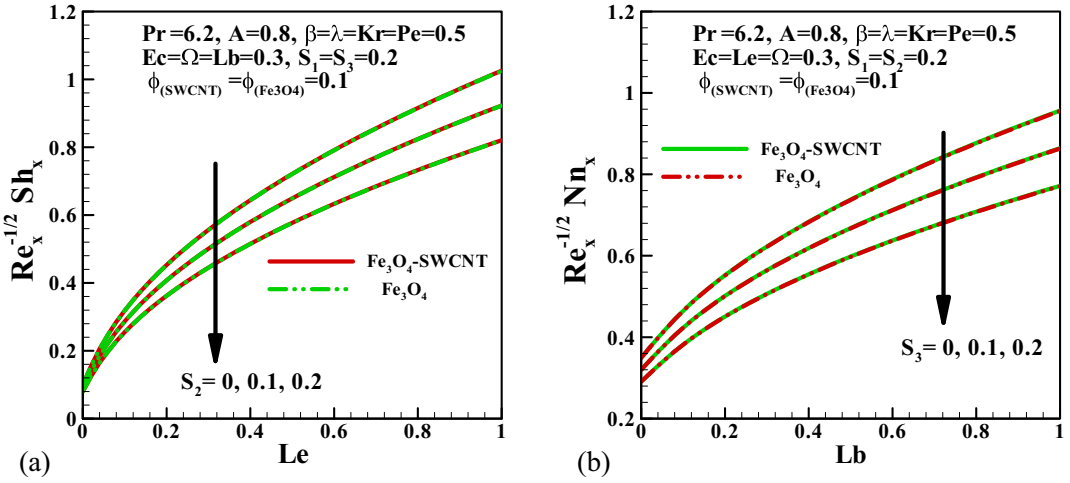

Fig. 14. Parallel effect of (*a*) S_2 *and Le* on $Sh_x\, Re_x^{-1/2}$ and (*b*) S_3 *and Lb* on $Nn_x\, Re_x^{-1/2}$.

$$\Upsilon_{11}{}' = \Upsilon_{12}$$

$$\Upsilon_{12}{}' = Pe\ \{\ (\Upsilon_{11} + \Omega)\ \Upsilon_{10}{}' + \Upsilon_{12}\ \Upsilon_{10}\ \} - Lb\ \Upsilon_1\ \Upsilon_{12}$$

with

$$\Upsilon_1(0) = 0, \Upsilon_2(0) = 1, \Upsilon_3(0) = \Gamma_1, \Upsilon_4(0) = 0$$

$$\Upsilon_5(0) = \Gamma_2, \Upsilon_6(0) = 0, \Upsilon_7(0) = 1 - S_1, \Upsilon_8(0) = \Gamma_3$$

$$\Upsilon_9(0) = 1 - S_2, \Upsilon_{10}(0) = \Gamma_4, \Upsilon_{11}(0) = 1 - S_3, \Upsilon_{12}(0) = \Gamma_5$$

where $\Gamma_1, \Gamma_2, \Gamma_3, \Gamma_4$ & Γ_5 are estimated using shooting technique with a suitable initial guess.Accuracy of the code and the validation of the current problem have been accounted for through a restrictive comparison of the present work with prior published works [21,46,47] (showcased in Table 1) and a commendable agreement is noted.

In proposed work, to simulate the flow for various values of parameters we have used MAPLE-17 software. The effects of the emerging parameters on the dimensionless velocity, temperature, skin friction, Nusselt number, mass transfer rate and microorganism density number are studied. The step size is taken $\Delta\zeta = 0.01$and accuracy is up to the fifth decimal place as the criterion of convergence. We assumed a suitable finite value for the far field boundary condition i.e.$\zeta \to \infty$, say ζ_∞. The iteration is done with the convergence criterion of 10^{-6} in all cases.

4. Results & discussion

The consequence of pertinent parameters on the physical quantities, microbial concentration ($\chi(\zeta)$), velocity ($f'(\zeta)$), concentration ($\psi(\zeta)$), temperature ($\theta(\zeta)$), and induced magnetic field ($g'(\zeta)$) profiles are depicted through Figs. 2 − 15. Studies have been carried out for water-based $Fe_3O_4 - SWCNT$ hybrid nanofluid & Fe_3O_4 nanofluid with Prandtl number (Pr) and infinity fixed at 6.2 and 10, respectively. Thermo-physical properties of the conventional fluid (water), Fe_3O_4 (nanoparticle 1), and SWCNT (nanoparticle 2) are showcased in Table 2.

Fig. 2(a) & (b) illustrate the impact of stretching parameter (A) on $f'(\zeta)$ & $g'(\zeta)$, respectively and it is perceived that augmenting A values produces a constructive effect on $f'(\zeta)$ and destructive effect on $g'(\zeta)$. Fig. 3 depicts the variations in $f'(\zeta)$ due to β (magnetic parameter). It is observed that $f'(\zeta)$ increases for augmenting β values when $A < 1$ and a reversed behaviour is observed for $f'(\zeta)$ when $A > 1$.

Fig. 4 bespeaks the deviation in $g'(\zeta)$ concerning β. An increase in $g'(\zeta)$ for $A < 1$ and a decrease $g'(\zeta)$ for $A > 1$ is noted for elevating β values. Fig. 5 explains the mixed effect of λ (reciprocal of magnetic Prandtl number) on $g'(\zeta)$. Initially, elevating λ values decays $g'(\zeta)$ and afterwards, a reversed trend is observed when $A < 1$. A similar but inversed impact is perceived when $A > 1$.

Figs. 6 & 7 elucidate the simultaneous effect of β, $\phi_{Fe_3O_4}$ & ϕ_{SWCNT} on $Cf_x\, Re_x^{1/2}$ (drag coefficient). It can be interpreted that $Cf_x\, Re_x^{1/2}$ improves with β and deteriorates with $\phi_{Fe_3O_4}$ & ϕ_{SWCNT} when $A < 1$. When $A > 1$,

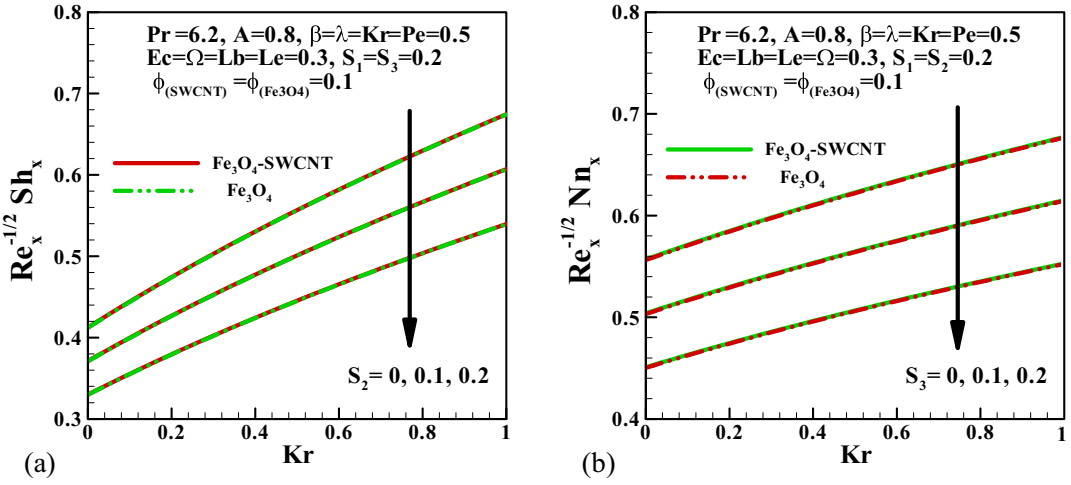

Fig. 15. Parallel effect of (*a*) S_2 *and Kr* on $Sh_x\ Re_x^{-1/2}$ and (*b*) S_3 *and Kr* on $Nn_x\ Re_x^{-1/2}$.

$Cf_x\ Re_x^{1/2}$ increases with $\phi_{Fe_3O_4}$ & ϕ_{SWCNT} and decreases with β. Biologically, a higher drag coefficient implies increased interaction between the fluid and the surface, which is beneficial in targeted drug delivery and biomedical imaging (see [38,48]).

Variation in $\theta(\zeta)$ due to $\phi_{Fe_3O_4}$ (volume fraction of nanoparticle 1) and ϕ_{SWCNT} (volume fraction of nanoparticle 2) are illustrated in Figs. 8(a) & 8(b), respectively. It is observed that $\theta(\zeta)$ ascends with augmenting $\phi_{Fe_3O_4}$ & ϕ_{SWCNT} values. Physically, this increase in temperature can be related to the improvement in the thermal conductivity of the nanoliquid caused by larger nanoparticle occupancy. The constructive effect of *Ec* (Eckert number) is illustrated in Fig. 9(b). Physically, it is associated with the generation of friction forces between the fluid particles which increases the temperature profile. In addition, the analysis on the significance of $\phi_{Fe_3O_4}$, ϕ_{SWCNT} & *Ec* on the temperature profile unveils that the nanoliquid can be used for killing tumors or cancerous cells (see [49]).

Fig. 9(a) depicts a descending nature of $\theta(\zeta)$ for S_1 (thermal stratification parameter). Physically, the decrease in the nanoliquid temperature is due to the decrease in the temperature difference between the surface and away from the surface caused by an increase in S_1. The simultaneous effect of *Ec*, S_1, $\phi_{Fe_3O_4}$ & ϕ_{SWCNT} on $Nu_x\ Re_x^{-1/2}$ (heat transfer rate) has been studied with the aid of Figs. 10 & 11. It can be said that for $A = 0.8$, $Nu_x\ Re_x^{-1/2}$ decreases with respect to S_1, *Ec* & ϕ_{SWCNT} and remains almost unchanged with respect to $\phi_{Fe_3O_4}$.

The stability to the problem involves finding the value range of the input parameter to keep the optimal solution unchanged, in this paper we have used various values of parameters where the solution is stable as mentioned in each figure.

Fig. 12 explains the consequence of *Kr* (chemical reaction parameter), *Le* (Lewis number) and S_2 (solutal stratification parameter) on $\psi(\zeta)$. A decreasing behaviour on the concentration profile is observed for augmenting *Kr*, *Le* & S_2 values. Physically, an increase in S_2 descends the concentration profile due to the decrease in the volumetric fraction between the surface and reference nanoparticles. Moreover, an increase in *Kr* consumes more nanoparticles and hence concentration decreases. Biologically, consumption of more nanoparticles is directly proportional to improved medication and biomedical imaging (see [50]). Fig. 13 discusses the impact of *Pe* (Peclet number) and S_3 (motile density stratification parameter) on $\chi(\zeta)$. It is observed that the augmenting effectual parameter values tend to decrease $\chi(\zeta)$. Physically, an augmentation in S_3 decreases the concentration difference of microorganisms between the surface and away from the surface and hence the microbial concentration decreases.

Figs. 14(a) & 15(a) bespeak the simultaneous variation of *Le*, *Kr* & S_2 on $Sh_x\ Re_x^{-1/2}$ (mass transfer rate) and Figs. 14(b) & 15(b) depict the simultaneous variation of *Lb* (bioconvection Lewis number), *Kr* & S_3 on $Nn_x\ Re_x^{-1/2}$ (microorganism density number). It can be easily observed that $Sh_x\ Re_x^{-1/2}$ increases with *Kr* & *Le* and decreases due to S_2. Furthermore, it is also noted that $Nn_x\ Re_x^{-1/2}$ increases with *Kr* & *Lb* and decreases due to S_3.

5. Conclusion

The dynamics of water conveying single-wall carbon nanotube and magnetite nanoparticles on the stagnation point flow along a stretching sheet subject to chemical reaction, viscous dissipation, induced magnetic field, and stratification effects have been numerically explored using the Runge-Kutta-Fehlberg method combined with the shooting technique. The key points noted from the study are:

- The augmenting volume fraction of single-wall carbon nanotube and magnetite nanoparticles raises the nanofluid temperature. Further, augmenting the Eckert number intensifies the nanofluid temperature. Biologically, the increase in the nanofluid temperature caused by the pertinent parameters is beneficial in killing tumors and cancerous cells.
- The velocity profile is directly proportional to the magnetic parameter when $A < 1$ and inversely proportional to the magnetic parameter when $A > 1$.
- The maximum drag coefficient (when $A = 0.8$) is experienced for higher values of the magnetic parameter and lower volume fraction of single-wall carbon nanotube and magnetite nanoparticles. However, the maximum drag coefficient (when $A = 1.2$) is experienced for lower values of the magnetic parameter and higher volume fraction of single-wall carbon nanotube and magnetite nanoparticles. Biologically, a higher drag coefficient implies increased interaction between the fluid and the surface, which is beneficial in targeted drug delivery and biomedical imaging.
- The mass transfer rate is a decreasing function of the solutal stratification parameter and an increasing function of the chemical reaction parameter.
- Augmenting chemical reaction parameter has a destructive effect on concentration profile that contributes towards improved medication and biomedical imaging.
- The microorganism density number is directly proportional to the chemical reaction parameter and is inversely proportional to the motile density stratification parameter.
- The maximum heat transfer rate is observed for smaller values of thermal stratification parameter, Eckert number, and nanoparticle volume fraction of single-wall carbon nanotube.

Declaration of Competing Interest

None.

Acknowledgement

The last author extend his appreciation to the Deanship of Scientific Research at King Khalid University for funding this work through General Research Program GRP/281/42.

References

[1] S.U.S. Choi, J.A. Eastman, Enhancing thermal conductivity of fluids with nanoparticles, in: Proc. 1995 Int. Mech. Eng. Congr. Expo 66, ASME, San Fr., 1995, pp. 99–105.
[2] A.S. Sabu, A. Mathew, T.S. Neethu, K. Anil George, Statistical analysis of MHD convective ferro-nanofluid flow through an inclined channel with hall current, heat source and soret effect, Therm. Sci. Eng. Prog. 22 (2021) 100816, https://doi.org/10.1016/j.tsep.2020.100816.
[3] A.S. Sabu, S. Areekara, A. Mathew, Statistical analysis on three-dimensional MHD convective Carreau nanofluid flow due to bilateral nonlinear stretching sheet with heat source and zero mass flux condition, Heat Transf. 50 (2021) 3641–3660, https://doi.org/10.1002/htj.22045.
[4] T.S. Neethu, S. Areekara, A. Mathew, Statistical approach on 3D hydromagnetic flow of water-based nanofluid between two vertical porous plates moving in opposite directions, Heat Transf. (2021), https://doi.org/10.1002/htj.22120.
[5] A.S. Sabu, S. Areekara, A. Mathew, Effects of multislip and distinct heat source on MHD Carreau nanofluid flow past an elongating cylinder using the statistical method, Heat Transf. (2021), https://doi.org/10.1002/htj.22142.
[6] F. Mabood, T.A. Yusuf, W.A. Khan, Cu–Al2O3–H2O hybrid nanofluid flow with melting heat transfer, irreversibility analysis and nonlinear thermal radiation, J. Therm. Anal. Calorim. (2020), https://doi.org/10.1007/s10973-020-09720-w.
[7] T.A. Yusuf, F. Mabood, W.A. Khan, J.A. Gbadeyan, Irreversibility analysis of cu-TiO2-H2O hybrid-nanofluid impinging on a 3-D stretching sheet in a porous medium with nonlinear radiation: Darcy-Forchhiemer's model, Alexandria Eng. J. 59 (2020) 5247–5261, https://doi.org/10.1016/j.aej.2020.09.053.
[8] S. Jakeer, P. Bala Anki Reddy, Entropy generation on EMHD stagnation point flow of hybrid nanofluid over a stretching sheet: homotopy perturbation solution, Phys. Scr. 95 (2020) 125203, https://doi.org/10.1088/1402-4896/abc03c.
[9] N.A. Zainal, R. Nazar, K. Naganthran, I. Pop, Unsteady EMHD stagnation point flow over a stretching/shrinking sheet in a hybrid Al2O3-cu/H2O nanofluid, Int. Commun. Heat Mass Transf. 123 (2021) 105205, https://doi.org/10.1016/j.icheatmasstransfer.2021.105205.
[10] F. Mabood, G.P. Ashwinkumar, N. Sandeep, Simultaneous results for unsteady flow of MHD hybrid nanoliquid above a flat/slendering surface, J. Therm. Anal. Calorim. (2020), https://doi.org/10.1007/s10973-020-09943-x.
[11] N. Acharya, F. Mabood, On the hydrothermal features of radiative Fe3O4–graphene hybrid nanofluid flow over a slippery bended surface with heat source/sink, J. Therm. Anal. Calorim. 143 (2021) 1273–1289, https://doi.org/10.1007/s10973-020-09850-1.
[12] F. Mabood, G.P. Ashwinkumar, N. Sandeep, Effect of nonlinear radiation on 3D unsteady MHD stagnancy flow of Fe3O4/graphene–water hybrid nanofluid, Int. J. Ambient Energy (2020), https://doi.org/10.1080/01430750.2020.1831593.
[13] O.K. Koriko, A.J. Omowaye, I.L. Animasaun, M.E. Bamisaye, Melting heat transfer and induced-magnetic field effects on the micropolar fluid flow towards stagnation point: boundary layer analysis, Int. J. Eng. Res. Afr. 29 (2017) 10–20, https://doi.org/10.4028/www.scientific.net/JERA.29.10.
[14] M. Kumari, H.S. Takhar, G. Nath, MHD flow and heat transfer over a stretching surface with prescribed wall temperature or heat flux, Wäarme- Und Stoffübertragung 25 (1990) 331–336.
[15] F.M. Ali, R. Nazar, N.M. Arifin, I. Pop, MHD boundary layer flow and heat transfer over a stretching sheet with induced magnetic field, Heat Mass Transf. 47 (2011) 155–162, https://doi.org/10.1007/s00231-010-0693-4.
[16] Z. Iqbal, E.N. Maraj, E. Azhar, Z. Mehmood, Framing the performance of induced magnetic field and entropy generation on cu and TiO2 nanoparticles by using Keller box scheme, Adv. Powder Technol. 28 (2017) 2332–2345, https://doi.org/10.1016/j.apt.2017.06.015.
[17] F.M. Ali, R. Nazar, N.M. Arifin, I. Pop, MHD stagnation-point flow and heat transfer towards stretching sheet with induced magnetic field, Appl. Math. Mech. English Ed. 32 (2011) 409–418, https://doi.org/10.1007/s10483-011-1426-6.
[18] T.R. Mahapatra, A.S. Gupta, Heat transfer in stagnation-point flow towards a stretching sheet, Heat Mass Transf. 38 (2002) 517–521, https://doi.org/10.1007/s002310100215.
[19] M.M. Junoh, F.M. Ali, N.M. Arifin, N. Bachok, I. Pop, MHD stagnation-point flow and heat transfer past a stretching/shrinking sheet in a hybrid nanofluid with induced magnetic field, Int. J. Numer. Methods Heat Fluid Flow 30 (2019) 1345–1364, https://doi.org/10.1108/HFF-06-2019-0500.
[20] M.I. Khan, T. Hayat, F. Shah, F. Haq Mujeeb-Ur-Rahman, Physical aspects of CNTs and induced magnetic flux in stagnation point flow with quartic chemical reaction, Int. J. Heat Mass Transf. 135 (2019) 561–568, https://doi.org/10.1016/j.ijheatmasstransfer.2019.01.141.
[21] Z. Iqbal, E. Azhar, E.N. Maraj, Transport phenomena of carbon nanotubes and bioconvection nanoparticles on stagnation point flow in presence of induced magnetic field, Phys. E Low Dimens. Syst. Nanostruct. 91 (2017) 128–135, https://doi.org/10.1016/j.physe.2017.04.022.
[22] M.K. Nayak, F. Mabood, A.S. Dogonchi, W.A. Khan, Electromagnetic flow of SWCNT/MWCNT suspensions with optimized entropy generation and cubic auto catalysis chemical reaction, Int. Commun. Heat Mass Transf. 104996 (2020), https://doi.org/10.1016/j.icheatmasstransfer.2020.104996.
[23] M.R. Eid, F. Mabood, Entropy analysis of a hydromagnetic micropolar dusty carbon NTs-kerosene nanofluid with heat generation: Darcy–Forchheimer scheme, J. Therm. Anal. Calorim. (2020), https://doi.org/10.1007/s10973-020-09928-w.
[24] S.Z. Abbas, M.K. Nayak, F. Mabood, A.S. Dogonchi, Y.-M. Chu, W.A. Khan, Darcy Forchheimer electromagnetic stretched flow of carbon nanotubes over an inclined cylinder: entropy optimization and quartic chemical reaction, Math. Methods Appl. Sci. (2020) 1–23, https://doi.org/10.1002/mma.6956.
[25] M.K. Nayak, F. Mabood, I. Tlili, A.S. Dogonchi, W.A. Khan, Entropy optimization analysis on nonlinear thermal radiative electromagnetic Darcy–Forchheimer flow of SWCNT/MWCNT nanomaterials, Appl. Nanosci. (2020), https://doi.org/10.1007/s13204-020-01611-8.
[26] H. Berrehal, F. Mabood, O.D. Makinde, Entropy-optimized radiating water/FCNTs nanofluid boundary-layer flow with convective condition, Eur. Phys. J. Plus 135 (2020), https://doi.org/10.1140/epjp/s13360-020-00536-z.
[27] H. He, L.A. Pham-Huy, P. Dramou, D. Xiao, P. Zuo, C. Pham-Huy, Carbon nanotubes: applications in pharmacy and medicine, Biomed. Res. Int. 2013 (2013) 578290, https://doi.org/10.1155/2013/578290.
[28] Z. Mehmood, Z. Iqbal, Interaction of induced magnetic field and stagnation point flow on bioconvection nanofluid submerged in gyrotactic microorganisms, J. Mol. Liq. 224 (2016) 1083–1091, https://doi.org/10.1016/j.molliq.2016.10.014.
[29] F. Al-Amri, M. Muthtamilselvan, Stagnation point flow of nanofluid containing micro-organisms, Case Stud. Therm. Eng. 21 (2020) 100656, https://doi.org/10.1016/j.csite.2020.100656.
[30] S. Ahmad, S. Nadeem, N. Muhammad, A. Issakhov, Radiative SWCNT and MWCNT nanofluid flow of Falkner–Skan problem with double stratification, Phys. A Stat. Mech. Appl. 547 (2020) 124054, https://doi.org/10.1016/j.physa.2019.124054.
[31] N.S. Khashi'ie, N.M. Arifin, M.M. Rashidi, E.H. Hafidzuddin, N. Wahi, Magnetohydrodynamics (MHD) stagnation point flow past a shrinking/stretching surface with double stratification effect in a porous medium, J. Therm. Anal. Calorim. 139 (2020) 3635–3648, https://doi.org/10.1007/s10973-019-08713-8.
[32] M.F.M. Basir, M.E.H. Hafidzuddin, K. Naganthran, S.S. Chaharborj Hashim, M.S. M. Kasihmuddin, R. Nazar, Stability analysis of unsteady stagnation-point gyrotactic bioconvection flow and heat transfer towards the moving sheet in a nanofluid, Chin. J. Phys. 65 (2020) 538–553, https://doi.org/10.1016/j.cjph.2020.02.021.
[33] P. Sudarsana Reddy, P. Sreedevi, Impact of chemical reaction and double stratification on heat and mass transfer characteristics of nanofluid flow over porous stretching sheet with thermal radiation, Int. J. Ambient Energy (2020), https://doi.org/10.1080/01430750.2020.1712240.
[34] A. Abbasi, W. Farooq, I. Riaz, Stagnation point flow of Maxwell nanofluid containing gyrotactic micro-organism impinging obliquely on a convective surface, Heat Transf. 49 (2020) 2977–2999, https://doi.org/10.1002/htj.21756.
[35] B. Blasiak, F.C.J.M. van Veggel, B. Tomanek, Applications of nanoparticles for MRI cancer diagnosis and therapy, J. Nanomater. 148578 (2013), https://doi.org/10.1155/2013/148578.
[36] J.P. Raval, P. Joshi, D.R. Chejara, 9 - Carbon nanotube for targeted drug delivery, in: Appl. Nanocomposite Mater. Drug Deliv, Woodhead Publishing, 2018, pp. 203–216, https://doi.org/10.1016/B978-0-12-813741-3.00009-1.
[37] M. Martincic, G. Tobias, Filled carbon nanotubes in biomedical imaging and drug delivery, Expert Opin. Drug Deliv. 12 (2015) 563–581, https://doi.org/10.1517/17425247.2015.971751.
[38] R.G. Bai, K. Muthoosamy, S. Manickam, Chapter 12 - Nanomedicine in theranostics, in: Nanotechnol. Appl. Tissue Eng, William Andrew Publishing, Oxford, 2015, pp. 195–213, https://doi.org/10.1016/B978-0-323-32889-0.00012-1.
[39] R.S. Kalash, V.K. Lakshmanan, C.-S. Cho, I.-K. Park, 4.4 - Theranostics, in: Biomater. Nanoarchitectonics, William Andrew Publishing, 2016, pp. 197–215, https://doi.org/10.1016/B978-0-323-37127-8.00012-1.
[40] E.J. Comparetti, V.A. de Pedrosa, R. Kaneno, Carbon nanotube as a tool for fighting cancer, Bioconjug. Chem. 29 (2018) 709–718, https://doi.org/10.1021/acs.bioconjchem.7b00563.
[41] K. Łukasiewicz, M. Fol, Microorganisms in the treatment of cancer: advantages and limitations, J Immunol Res 2397808 (2018), https://doi.org/10.1155/2018/2397808.
[42] A. Alsaedi, M.I. Khan, M. Farooq, N. Gull, T. Hayat, Magnetohydrodynamic (MHD) stratified bioconvective flow of nanofluid due to gyrotactic microorganisms, Adv. Powder Technol. 28 (2017) 288–298, https://doi.org/10.1016/j.apt.2016.10.002.
[43] A. Tulu, W. Ibrahim, MHD slip flow of CNT-ethylene glycol nanofluid due to a stretchable rotating disk with Cattaneo – Christov heat flux model, Math. Probl. Eng. (2020), https://doi.org/10.1155/2020/1374658.
[44] P. Sreedevi, P. Sudarsana Reddy, Effect of SWCNTs and MWCNTs Maxwell MHD nanofluid flow between two stretchable rotating disks under convective boundary conditions, Heat Transf. Res. 48 (2019) 4105–4132, https://doi.org/10.1002/htj.21584.
[45] F. Saba, N. Ahmed, U. Khan, S.T. Mohyud-din, A novel coupling of (CNT-Fe3O4/H2O) hybrid nanofluid for improvements in heat transfer for flow in an asymmetric channel with dilating/squeezing walls, Int. J. Heat Mass Transf. 136 (2019) 186–195, https://doi.org/10.1016/j.ijheatmasstransfer.2019.02.097.

[46] T. Hayat, M. Farooq, A. Alsaedi, Homogeneous-heterogeneous reactions in the stagnation point flow of carbon nanotubes with Newtonian heating, AIP Adv. 5 (2015) 27130, https://doi.org/10.1063/1.4908602.
[47] T. Hayat, K. Muhammad, M. Farooq, A. Alsaedi, Melting heat transfer in stagnation point flow of carbon nanotubes towards variable thickness surface, AIP Adv. 6 (2016) 15214, https://doi.org/10.1063/1.4940932.
[48] R. Jamshidi, L. Mazzei, CFD modeling of fluidized beds, in: Ref. Modul. Chem. Mol. Sci. Chem. Eng, Elsevier, 2018, https://doi.org/10.1016/B978-0-12-409547-2.13698-4.
[49] M. Jama, T. Singh, S.M. Gamaleldin, M. Koc, A. Samara, R.J. Isaifan, M.A. Atieh, Critical review on nanofluids: preparation, characterization, and applications, J. Nanomater. 6717624 (2016), https://doi.org/10.1155/2016/6717624.
[50] P. Kaur, M.L. Aliru, A.S. Chadha, A. Asea, S. Krishnan, Hyperthermia using nanoparticles – promises and pitfalls, Int. J. Hyperth. 32 (2016) 76–88, https://doi.org/10.3109/02656736.2015.1120889.